Hindawi
Mathematical Problems in Engineering
Volume 2019, Article ID 7969371, 14 pages
https://doi.org/10.1155/2019/7969371

Research Article

Efficient Implementation and Numerical Analysis of Finite Element Method for Fractional Allen-Cahn Equation

Guozhen Wang and Huanzhen Chen

College of Mathematics and Statistics, Shandong Normal University, Jinan 250014, China

Correspondence should be addressed to Huanzhen Chen; chhzh@sdnu.edu.cn

Received 18 May 2019; Accepted 15 July 2019; Published 28 July 2019

Academic Editor: Chris Goodrich

We embed the fractional Allen-Cahn equation into a Galerkin variational framework and thus develop its corresponding finite element procedure and then prove rigorously its mathematical and physical properties for the finite element solution. Combining the merits of the conjugate gradient (CG) algorithm and the Toeplitz structure of the coefficient matrix, we design a fast CG for the linearized finite element scheme to reduce the computation cost and the storage to $O(M\log M)$ and $O(M)$, respectively. Numerical experiments confirm that the proposed fast CG algorithm recognizes accurately the mass and energy dissipation, the phase separation through a very clear coarse graining process, and the influences of different indices r of fractional Laplacian and different coefficients K, η on the width of the interfaces.

1. Introduction

As a typical phase-field model, the classical Allen-Cahn equation [1]

$$\partial_t u - K\Delta u + \psi'(u) = 0, \tag{1}$$

was originally derived through the minimization of the Ginzburg-Landau free energy functional

$$\int_\Omega \left(\frac{1}{2}|\nabla u|^2 + \psi(u)\right) dx \tag{2}$$

to describe the motion of antiphase boundaries in crystalline solids with the double-well potential $\psi(u) = (1/4\eta^2)(u^2 - 1)^2$. Since then, the Allen-Cahn equation has been widely applied to many complicated moving interface problems, for example, vesicle membranes, nucleation of solids, and mixture of two incompressible fluids, etc. (cf. [2–8]), and many and many research results on its theories, applications, and numerics of the Allen-Cahn equation have been achieved; see the reviews [9–15] and the references cited therein.

To recognize the influences of the long-range interactions between particles in those complicated moving interface problems, it could reasonably make physical significance if the Laplacian operator in (1) is replaced by its fractional version of Riesz-type potential to form the fractional Allen-Cahn equation. In this line, [16] proposed a kind of fractional Allen-Cahn model and discussed the solvability in some fractional Sobolev spaces, and [17] developed a fractional extension of the Allen-Cahn phase-field model with its fractional Laplacian defined by Riemann-Liouville fractional derivative that describes the mixture of two incompressible fluids. In [17], the authors also proposed a Petrov-Galerkin spectral method for spacial discretization combined with a stabilized ADI scheme for temporal discretization in the absence of rigorous numerical analysis for the solvability, stability, convergence, and conservation properties of the numerical scheme. Some other numerical methods such as finite difference [18], finite volume [19], and collocation method [20] were established. As far as we know, few research works have been done on the efficient finite element method and its rigorous numerical analysis for the fractional Laplace operator defined as Riesz-type potentials on the whole space R.

In this article, we consider the following fractional Allen-Cahn equation [16]:

$$\partial_t u + K\left[(-\Delta)^r u + \psi'(u)\right] = 0, \quad (x,t) \in \Omega \times (0,T],$$

$$u(x,0) = u^0(x), \quad x \in R,$$
$$u(x,t) = 0, \quad (x,t) \in \overline{\Omega} \times [0,T], \tag{3}$$

where $\Omega = (0,1)$, $r \in (0,1)$, $K > 0$ is the diffusion coefficient and the fractional Laplace operator $(-\Delta)^r$ is defined as Riesz-type potentials on the whole space R in Section 2. The unknown $u(x)$ can be viewed as an indicator of the concentration or volume fraction of one fluid at the location x in the immiscible mixture with the second fluid.

The main objectives of this article are to (1) embed the fractional Allen-Cahn equation (1) into a Galerkin variational framework and thus develop its corresponding finite element procedure; (2) prove rigorously the solvability, the optimal convergence rates, and the physical properties, for examples, the mass decay, the energy dissipation, and the new energy equality, for the finite element solution; (3) combine the Toeplitz structure of the coefficient matrix and the merits of the classic CG algorithm [21] to design a fast CG (FCG) for the linearized finite element scheme, which reduces the computation cost and the storage to $O(M \log M)$ and $O(M)$, respectively; and (4) conduct numerical experiments to verify the efficiency of the FCG, which show that the FCG possesses the ideal convergence rates as Newtons algorithm does in space and time, preserves the mass, energy dissipation, and energy equality law, and recognizes accurately the phase separation by a very clear coarse graining process. The numerical experiments also test the tunable sharpness, that is, the influences of different fractional indices r and different coefficients η.

The rest of this article is outlined as follows. Section 2 is preliminaries. Section 3 is for the solvability and stability of the solution of discrete system. We demonstrate that the discrete solution preserves mass and energy dissipation and satisfies new energy equality in Section 4. Sections 5 and 6 are devoted to convergence analysis and efficient FCG algorithm, respectively. In the last section, numerical experiments are conducted to test the efficiency of the proposed efficient finite element algorithm.

2. Preliminaries

We first briefly revisit the definitions and some properties of fractional Laplace operator.

Definition 1 (see [22, 23]). For $r \in (0,1)$ and $u \in \mathcal{S}(x)$, where $\mathcal{S}(x)$ is the Schwartz class of rapidly decaying functions at infinity, the fractional Laplace operator $(-\Delta)^r$ is reformulated by

$$(-\Delta)^r u(x) := C_r \lim_{\epsilon \longrightarrow 0} \int_{R \backslash B(x,\epsilon)} \frac{u(x) - u(y)}{|x-y|^{1+2r}} dy, \tag{4}$$

where C_r is a constant given by

$$C_r = \frac{4^r r \Gamma(1/2 + r)}{\pi^{1/2} \Gamma(1-r)}. \tag{5}$$

Definition 2 (see [22, 24, 25]). For $0 < r < 1$, the fractional Sobolev spaces $H_0^r(R)$ are defined by

$$L_0^2(R) := \left\{ v \in L^2(R) : v = 0 \text{ in } R \backslash \Omega \right\},$$
$$H_0^r(R) := \left\{ v \in L_0^2(R) : \frac{|v(x) - v(y)|^2}{|x-y|^{1+2r}} \in L^1(R \times R) \right\} \tag{6}$$

and equipped with the norm

$$\|v\|_{H^r(R)}^2 := \|v\|_{L^2(R)}^2 + \frac{C_r}{2} \int_R \int_R \frac{|v(x) - v(y)|^2}{|x-y|^{1+2r}} dxdy, \quad v \in H_0^r(R). \tag{7}$$

and with equivalent seminorm

$$|v|_{H^r(R)}^2 := \frac{C_r}{2} \int_R \int_R \frac{|v(x) - v(y)|^2}{|x-y|^{1+2r}} dxdy, \quad v \in H_0^r(R). \tag{8}$$

The energy space and the energy are defined, respectively, by

$$\mathbb{H}_r(R) := \left\{ v \in H_0(R) : \mathbb{E}_r(v) < +\infty \right\}, \tag{9}$$

$$\mathbb{E}_r(v) := \frac{K}{2} \|v\|_{H_0^r}^2 + \frac{K}{4\eta^2} \int_R v^4 dx - \frac{K}{2\eta^2} \int_R v^2 dx, \quad \forall v \in H_0^r(R). \tag{10}$$

Definition 3 (see [22]). For $0 < r < 1$, the operator $T_r : H_0^r(R) \longrightarrow H_0^{lr}(R)$ is defined by

$$\langle T_r u, v \rangle_{H_0^r} := \frac{C_r}{2} \int_R \int_R \frac{(u(x) - u(y))(v(x) - v(y))}{|x-y|^{1+2r}} dxdy, \quad \forall u, v \in H_0^r. \tag{11}$$

Here $H_0^{lr}(R)$ stands for its dual of $H_0^r(R)$.

It is easily seen that T_r is a symmetric positive definite operator.

Definition 4 (see [22]). Let $T > 0$. If $u \in C([0,T]; H_0^r) \cap W^{1,2}([0,T]; H_0^{lr})$ satisfies

$$\partial_t u + K \left[(-\Delta)^r u + \frac{1}{\eta^2} \left(u^3 - u \right) \right] = 0, \quad a.e. \text{ in } H_0^{lr}, \tag{12}$$

then the u is called a weak solution to problem (3).

3. Finite Element Procedure

In this section, we construct finite element scheme for (3) based on the weak formulation (12) and prove the solvability and stability of solution of discrete system.

Multiplying (12) by any $v \in H_0^r$, integrating over R and combining the homogeneous boundary condition, we obtain the variational formulation of (3) as to find $u \in H_0^r$ such that

$$(a)\ \left(\partial_t u, v\right) + K\left\langle T_r u, v\right\rangle + \frac{K}{\eta^2}\left(u^3, v\right) - \frac{K}{\eta^2}(u, v) = 0, \quad \forall v \in H_0^r, \tag{13}$$

$$(b)\ u(x,0) = u^0(x).$$

Taking M and N as integers, we divide $\Omega = [0,1]$ uniformly by intervals $I_i = [x_{i-1}, x_i]$ for $i = 1, 2, \ldots, M$ with $x_0 = 0$, $x_M = 1$, $h = h_i = x_i - x_{i-1} = 1/M$, and partition the time interval $[0,T]$ by the nodes $t_n = n\tau$ for $n = 0, 1, \ldots, N$ with the time step $\tau = T/N$.

Upon the space partition, we define the finite element space as

$$V_h := \left\{v_h \in C(\Omega) : v_h\big|_{I_i} \in P_k(I_i),\ i = 1, 2, \ldots, M;\ v_h(0) = v_h(1) = 0;\ k \geq 1\right\}, \tag{14}$$

here $P_k(I_i)$ being the set of polynomials of degree not bigger than k over the interval I_i.

Applying the backward Euler scheme to discrete the time derivative $\partial_t u$, we define the fully discrete finite element procedure of (13) as to find $u_h^n \in V_h$ such that, for $v_h \in V_h$,

$$(a)\ \left(\frac{u_h^n - u_h^{n-1}}{\tau}, v_h\right) + K\left\langle T_r u_h^n, v_h\right\rangle + \frac{K}{\eta^2}\left(\left(u_h^n\right)^3, v_h\right) - \frac{K}{\eta^2}\left(u_h^n, v_h\right) = 0, \tag{15}$$

$$(b)\ u_h^0 = R_h u^0,$$

where $R_h u^0$ is the elliptic projection of the initial value $u^0(x)$ to the finite element space.

The dimension of V_h is $(kM-1)\times(kM-1)$; see the review [24]. Assume $\varphi_i(x), i = 1, 2, \ldots, kM-1$ are the basis functions; then, we can express the numerical solution u_h^n by

$$u_h^n(x) = \sum_{i=1}^{kM-1} u_i^n \varphi_i(x), \tag{16}$$

and, thus, the fully discrete finite element scheme (15) is transformed equivalently to the following algebraic equation:

$$\left(\left(1 - \frac{\tau K}{\eta^2}\right)A + \tau K B\right)U^n + \frac{\tau K}{\eta^2} H\left(U^n\right)U^n = AU^{n-1}, \tag{17}$$

where $U^n = (u_1^n, u_2^n, \ldots, u_{kM-1}^n)^T$ is the unknown vector, and the matrices $A, B, H(U^n)$ are

$$A = \left[\left(\varphi_i, \varphi_j\right)\right]_{(kM-1)\times(kM-1)},$$
$$B = \left[\left\langle T_r\varphi_i, \varphi_j\right\rangle\right]_{(kM-1)\times(kM-1)}, \tag{18}$$
$$H\left(U^n\right) = \left[\left(\left(u_h^n\right)^2 \varphi_i, \varphi_j\right)\right]_{(kM-1)\times(kM-1)}.$$

It is easily verified that A, B, and $H(U^n)$ are symmetric and positive matrices.

By using the contraction mapping principle, we prove the existence and uniqueness of the fully discrete finite element scheme (15).

Theorem 5. *There exists a unique solution $U^n, n = 1, 2, \ldots, N$ to (17) for sufficiently small $\tau > 0$.*

Proof. Selecting the time step τ sufficiently small such that $0 < \tau CK/\eta^2 < 1$ and noticing that $\tau K > 0$ and the matrices A and B are positive definite, we know that the matrix

$$E := \left(1 - \frac{\tau K}{\eta^2}\right)A + \tau K B \tag{19}$$

is positive definite and thus invertible for sufficiently small $\tau > 0$. Therefore, we solve U^n from (17)

$$U^n = -E^{-1}\frac{\tau K}{\eta^2} H\left(U^n\right)U^n + E^{-1}AU^{n-1}. \tag{20}$$

Define the mapping $\mathcal{T}: X \in R^{kM-1} \longrightarrow Y \in R^{kM-1}$ by

$$Y = -E^{-1}\frac{\tau K}{\eta^2} H(X)X + E^{-1}AU^{n-1}. \tag{21}$$

The mapping $\mathcal{T}$ is well defined for given U^{n-1} due to the positiveness of the matrix E.

We shall use a corollary of the well-known contraction mapping principle [26] to prove the mapping $\mathcal{T}$ having a unique fixed point in a bounded domain $\mathcal{U} = \{X \in R^{kM-1}; \|X\| \leq L\}$ of R^{kM-1}.

For this purpose, we let $X_i \in \mathcal{U}$ and $Y_i = T(X_i)$ for $i = 1, 2$. Then,

$$\begin{aligned}\left\|Y_1 - Y_2\right\| &= \left\|\mathcal{T}(X_1) - \mathcal{T}(X_2)\right\| \\ &= \left\|-\frac{\tau K}{\eta^2}E^{-1}\left(H(X_1)X_1 - H(X_2)X_2\right)\right\|.\end{aligned} \tag{22}$$

Noticing that the matrix $H(X)$ is Lipschitz continuously with respect to X, we obtain

$$\begin{aligned}\left\|Y_1 - Y_2\right\| &\leq \frac{\tau K}{\eta^2}\left\|E^{-1}\right\|\left\|\left(H(X_1)X_1 - H(X_2)X_2\right)\right\| \\ &\leq \frac{\tau K}{\eta^2}\left\|E^{-1}\right\|\left(\left\|H(X_1)\right\|\left\|X_1 - X_2\right\|\right. \\ &\quad \left. + \left\|H(X_1) - H(X_2)\right\|\left\|X_2\right\|\right) \leq \frac{\tau K}{\eta^2}\left\|E^{-1}\right\| \\ &\quad \cdot\left(\left\|H(X_1)\right\|\left\|X_1 - X_2\right\| + C\left\|X_1 - X_2\right\|\left\|X_2\right\|\right) \\ &= \frac{\tau K}{\eta^2}\left\|E^{-1}\right\|\left(\left\|H(X_1)\right\| + C\left\|X_2\right\|\right)\left\|X_1 - X_2\right\| \\ &\leq \frac{\tau K}{\eta^2}\left\|E^{-1}\right\|\sup_{X_1, X_2 \in \mathcal{U}}\left(\left\|H(X_1)\right\| + C\left\|X_2\right\|\right)\left\|X_1 - X_2\right\|.\end{aligned} \tag{23}$$

Select τ to be small enough such that

$$0 < \tau < \left(\frac{K}{\eta^2} \left\| E^{-1} \right\| \sup_{X_1, X_2 \in \mathscr{U}} \left(\left\| H\left(X_1\right) \right\| + C \left\| X_2 \right\| \right) \right)^{-1}, \quad (24)$$

and we have

$$\left\| Y_1 - Y_2 \right\| < \left\| X_1 - X_2 \right\|, \quad (25)$$

which shows that the mapping $\mathscr{T}$ is a contractive mapping. This, together with an application of the well-known contraction mapping principle, completes the proof. □

Theorem 6. *Assume that τ is small enough such that the conditions of Theorem 5 hold. Then, the fully discrete finite element scheme (15) is stable in the following sense, for $J = 1, 2, \ldots, N$,*

$$\begin{aligned} &\left\| u_h^J \right\|^2 + 2\tau K \sum_{i=1}^{J} \left| u_h^i \right|_{H_r}^2 + \frac{2\tau K}{\eta^2} \sum_{i=1}^{J} \left\| u_h^i \right\|_{L_4}^4 \\ &\quad \le e^{2KT/\eta^2} \left\| u_h^0 \right\|^2. \end{aligned} \quad (26)$$

Proof. Take $v_h = u_h^n$ in (15) to obtain

$$\begin{aligned} &(a) \left(\frac{u_h^n - u_h^{n-1}}{\tau}, u_h^n \right) + K \left\langle T_r u_h^n, u_h^n \right\rangle \\ &\quad + \frac{K}{\eta^2} \left(\left(u_h^n\right)^3, u_h^n \right) - \frac{K}{\eta^2} \left(u_h^n, u_h^n \right) = 0, \\ &(b)\ u_0^h = R_h u_0. \end{aligned} \quad (27)$$

Noting the fact that

$$\begin{aligned} \left\langle T_r u_h^n, u_h^n \right\rangle &= \left| u_h^i \right|_{H_r}^2, \\ \left(\left(u_h^n\right)^3, u_h^n \right) &= \left\| u_h^n \right\|_{L_4}^4 \end{aligned} \quad (28)$$

and

$$\left(u_h^n - u_h^{n-1}, u_h^n \right) \ge \frac{1}{2} \left\| u_h^n \right\|^2 - \frac{1}{2} \left\| u_h^{n-1} \right\|^2, \quad (29)$$

we have

$$\begin{aligned} &\left\| u_h^n \right\|^2 - \left\| u_h^{n-1} \right\|^2 + 2\tau K \left| u_h^i \right|_{H_r}^2 \\ &\quad + \frac{2\tau K}{\eta^2} \left(\left\| u_h^n \right\|_{L_4}^4 - \left\| u_h^n \right\|^2 \right) \le 0. \end{aligned} \quad (30)$$

Adding all the terms from $n = 1$ to $n = J$, we get

$$\begin{aligned} &\left\| u_h^J \right\|^2 - \left\| u_h^0 \right\|^2 + 2\tau K \sum_{i=1}^{J} \left| u_h^i \right|_{H_r}^2 \\ &\quad + \frac{2\tau K}{\eta^2} \left(\sum_{i=1}^{J} \left\| u_h^i \right\|_{L_4}^4 - \sum_{i=1}^{J} \left\| u_h^i \right\|^2 \right) \le 0. \end{aligned} \quad (31)$$

Namely,

$$\begin{aligned} &\left\| u_h^J \right\|^2 + 2\tau K \sum_{i=1}^{J} \left| u_h^i \right|_{H_r}^2 + \frac{2\tau K}{\eta^2} \sum_{i=1}^{J} \left\| u_h^i \right\|_{L_4}^4 \\ &\quad \le \frac{2\tau K}{\eta^2} \sum_{i=1}^{J} \left\| u_h^i \right\|^2 + \left\| u_h^0 \right\|^2. \end{aligned} \quad (32)$$

Applying the discrete Gronwall inequality, we have

$$\begin{aligned} &\left\| u_h^J \right\|^2 + 2\tau K \sum_{i=1}^{J} \left| u_h^i \right|_{H_r}^2 + \frac{2\tau K}{\eta^2} \sum_{i=1}^{J} \left\| u_h^i \right\|_{L_4}^4 \\ &\quad \le e^{J(2\tau K/\eta^2)} \left\| u_h^0 \right\|^2 \le e^{2TK/\eta^2} \left\| u_h^0 \right\|^2. \end{aligned} \quad (33)$$

This completes the proof. □

4. Properties Preserved by the Finite Element Solution

In this section, we demonstrate that the finite element solution preserves the energy dissipation law and satisfies a redefined energy equality.

Theorem 7. *The finite element solution u_h^n of (15) preserves the energy dissipation law in the following sense, for $J = 1, 2, \ldots, N$,*

$$\mathbb{E}_r\left(u_h^J\right) \le \mathbb{E}_r\left(u_h^{J-1}\right) \le \cdots \le \mathbb{E}_r\left(u^0\right). \quad (34)$$

Proof. Taking $v_h = (u_h^n - u_h^{n-1})/\tau$ in (15), we have

$$\begin{aligned} &\left(\frac{u_h^n - u_h^{n-1}}{\tau}, \frac{u_h^n - u_h^{n-1}}{\tau} \right) + K \left\langle T_r u_h^n, \frac{u_h^n - u_h^{n-1}}{\tau} \right\rangle \\ &\quad + \frac{K}{\eta^2} \left(\left(u_h^n\right)^3, \frac{u_h^n - u_h^{n-1}}{\tau} \right) \\ &\quad - \frac{K}{\eta^2} \left(u_h^n, \frac{u_h^n - u_h^{n-1}}{\tau} \right) = 0. \end{aligned} \quad (35)$$

Due to the fact that

$$\begin{aligned} \left\| u_h^n \right\|_{L^2}^2 &= \left(u_h^n, u_h^n \right) = \left(U^n\right)^T A U^n, \\ \left\| u_h^n \right\|_{H^r}^2 &= \left\langle T_r u^n, u^n \right\rangle = \left(U^n\right)^T B U^n, \end{aligned} \quad (36)$$

we have

$$\begin{aligned} \left(u_h^n, u_h^n - u_h^{n-1} \right) &= \left(U^n\right)^T A \left(U^n - U^{n-1} \right) \\ &\ge \frac{1}{2} \left(\left(U^n\right)^T A U^n - \left(U^{n-1}\right)^T A U^{n-1} \right) \end{aligned} \quad (37)$$

and

$$\begin{aligned} \left\langle T_r u_h^n, u_h^n - u_h^{n-1} \right\rangle &= \left(U^n\right)^T B \left(U^n - U^{n-1} \right) \\ &\ge \frac{1}{2} \left(\left(U^n\right)^T B U^n - \left(U^{n-1}\right)^T B U^{n-1} \right). \end{aligned} \quad (38)$$

By applying the inequality $ab \le (1/2)(a^2 + b^2)$, we get

$$\begin{aligned}\left(\left(u_h^n\right)^3, u_h^n - u_h^{n-1}\right) &= \left(\left(u_h^n\right)^2, u_h^n\left(u_h^n - u_h^{n-1}\right)\right)\\ &\ge \frac{1}{2}\left(\left(u_h^n\right)^2, \left(u_h^n\right)^2 - \left(u_h^{n-1}\right)^2\right)\\ &\ge \frac{1}{4}\left(\left(u_h^n\right)^4 - \left(u_h^{n-1}\right)^4, 1\right).\end{aligned} \tag{39}$$

Then, combining the above inequalities with (35), we derive

$$\begin{aligned}&\tau\left\|\frac{u_h^n - u_h^{n-1}}{\tau}\right\|^2 + \frac{K}{2}\left(\left|u_h^n\right|_{H^r}^2 - \left|u_h^{n-1}\right|_{H^r}^2\right)\\ &\quad + \frac{K}{4\eta^2}\left(\left\|u_h^n\right\|_{L^4}^4 - \left\|u_h^{n-1}\right\|_{L^4}^4\right)\\ &\quad - \frac{K}{2\eta^2}\left(\left\|u_h^n\right\|^2 - \left\|u_h^{n-1}\right\|^2\right) \le 0.\end{aligned} \tag{40}$$

Therefore, we have

$$\begin{aligned}&\frac{K}{2}\left|u_h^n\right|_{H^r}^2 + \frac{K}{4\eta^2}\left\|u_h^n\right\|_{L^4}^4 - \frac{K}{2\eta^2}\left\|u_h^n\right\|^2\\ &\le \frac{K}{2}\left|u_h^{n-1}\right|_{H^r}^2 + \frac{K}{4\eta^2}\left\|u_h^{n-1}\right\|_{L^4}^4 - \frac{K}{2\eta^2}\left\|u_h^{n-1}\right\|^2.\end{aligned} \tag{41}$$

It follows that $\mathbb{E}_r(u_h^n) \le \mathbb{E}_r(u_h^{n-1})$ for $n = 1, \ldots, J$. This completes the proof. □

We prove the following new energy equality preserved by the finite element solution u_h.

Theorem 8. *The finite element solution u_h^n of (15) satisfies the following energy equality for $J = 1, 2, \ldots, N$,*

$$\begin{aligned}&E_r\left(u_h^J\right) + \frac{1}{\tau}\sum_{i=1}^{J}\left\|u_h^i - u_h^{i-1}\right\|^2 + \frac{K}{2\eta^2}\sum_{i=1}^{J}\left|u_h^i - u_h^{i-1}\right|_{H^r}^2\\ &\quad + \frac{K}{4\eta^2}\sum_{i=1}^{J}\left\|\left(u_h^i\right)^2 - \left(u_h^{i-1}\right)^2\right\|^2\\ &\quad + \frac{K}{2\eta^2}\sum_{i=1}^{J}\left\|\left(u_h^i\right)^2 - u_h^i u_h^{i-1}\right\|^2\\ &\quad - \frac{K}{2\eta^2}\sum_{i=1}^{J}\left\|u_h^i - u_h^{i-1}\right\|^2 = E_r\left(u_h^0\right),\end{aligned} \tag{42}$$

where the left-hand side of the energy equality (42) is redefined as the new energy.

Proof. Choosing $(u_h^n - u_h^{n-1})/\tau$ and multiplying τ^2 to both sides in (15), we get

$$\begin{aligned}&\left(u_h^n - u_h^{n-1}, u_h^n - u_h^{n-1}\right) + \tau K\left\langle T_r u_h^n, u_h^n - u_h^{n-1}\right\rangle\\ &\quad + \frac{\tau K}{\eta^2}\left(\left(u_h^n\right)^3, u_h^n - u_h^{n-1}\right) - \frac{\tau K}{\eta^2}\left(u_h^n, u_h^n - u_h^{n-1}\right)\\ &= 0.\end{aligned} \tag{43}$$

By a simple calculation, we have

$$\begin{aligned}\left\langle T_r u_h^n, u_h^n - u_h^{n-1}\right\rangle &= \frac{1}{2}\left|u_h^n\right|_{H^r}^2 - \frac{1}{2}\left|u_h^{n-1}\right|_{H^r}^2\\ &\quad + \frac{1}{2}\left|u_h^n - u_h^{n-1}\right|_{H^r}^2,\\ \left(u_h^n, u_h^n - u_h^{n-1}\right) &= \frac{1}{2}\left\|u_h^n\right\|^2 - \frac{1}{2}\left\|u_h^{n-1}\right\|^2\\ &\quad + \frac{1}{2}\left\|u_h^n - u_h^{n-1}\right\|^2\end{aligned} \tag{44}$$

and

$$\begin{aligned}\left(\left(u_h^n\right)^3, u_h^n - u_h^{n-1}\right) &= \frac{1}{4}\left\|u_h^n\right\|_{L_4}^4 - \frac{1}{4}\left\|u_h^{n-1}\right\|_{L_4}^4\\ &\quad + \frac{1}{4}\left\|\left(u_h^n\right)^2 - \left(u_h^{n-1}\right)^2\right\|^2\\ &\quad + \frac{1}{2}\left\|\left(u_h^n\right)^2 - u_h^n u_h^{n-1}\right\|^2.\end{aligned} \tag{45}$$

Substituting the above equalities into (43) and combining (10), we have

$$\begin{aligned}&\tau E_r\left(u_h^n\right) - \tau E_r\left(u_h^{n-1}\right) + \left\|u_h^n - u_h^{n-1}\right\|^2\\ &\quad + \frac{\tau K}{2\eta^2}\left|u_h^n - u_h^{n-1}\right|_{H^r}^2 + \frac{\tau K}{4\eta^2}\left\|\left(u_h^n\right)^2 - \left(u_h^{n-1}\right)^2\right\|^2\\ &\quad + \frac{\tau K}{2\eta^2}\left\|\left(u_h^n\right)^2 - u_h^n u_h^{n-1}\right\|^2 - \frac{\tau K}{2\eta^2}\left\|u_h^n - u_h^{n-1}\right\|^2\\ &= 0.\end{aligned} \tag{46}$$

Add all terms from $n = 1$ to $n = J$ to obtain

$$\begin{aligned}&\tau E_r\left(u_h^J\right) + \sum_{i=1}^{J}\left\|u_h^i - u_h^{i-1}\right\|^2 + \frac{\tau K}{2\eta^2}\sum_{i=1}^{J}\left|u_h^i - u_h^{i-1}\right|_{H^r}^2\\ &\quad + \frac{\tau K}{4\eta^2}\sum_{i=1}^{J}\left\|\left(u_h^i\right)^2 - \left(u_h^{i-1}\right)^2\right\|^2\\ &\quad + \frac{\tau K}{2\eta^2}\sum_{i=1}^{J}\left\|\left(u_h^i\right)^2 - u_h^i u_h^{i-1}\right\|^2\\ &\quad - \frac{\tau K}{2\eta^2}\sum_{i=1}^{J}\left\|u_h^i - u_h^{i-1}\right\|^2 = \tau E_r\left(u_h^0\right).\end{aligned} \tag{47}$$

This completes the proof. □

5. Convergence Analysis

In this section, we shall conduct convergence analysis for the fully discrete finite element scheme (15).

Define the elliptic projection $R_h u$ of the exact solution u as

$$\left\langle T_r\left(u - R_h u\right), v_h\right\rangle = 0, \quad \forall v_h \in V_h. \tag{48}$$

The following estimate is valid for $u \in H^s(\Omega)$ and $s > r$ [27],

$$\left\|u - R_h u\right\|_r \le C h^{\min\{k+1-r, s-r\}} \|u\|_s . \tag{49}$$

Let $t = t_n$ and $v = v_h$ in (13), and subtract it from (15) to obtain the error equation

$$\begin{aligned} &(a)\ \left(u_t^n - \frac{u_h^n - u_h^{n-1}}{\tau}, v_h\right) + K\left\langle T_r\left(u^n - u_h^n\right), v_h\right\rangle \\ &\quad + \frac{K}{\eta^2}\left(\left(u^n\right)^3 - \left(u_h^n\right)^3, v_h\right) - \frac{K}{\eta^2}\left(u^n - u_h^n, v_h\right) = 0, \\ &\qquad\qquad \forall v_h \in V_h, \\ &(b)\ u_h^0 = R_h u^0. \end{aligned} \tag{50}$$

Denote

$$\begin{aligned} u_t^n - \frac{u^n - u^{n-1}}{\tau} &= S^n, \\ u^n - R_h u^n &= \rho^n, \\ R_h u^n - u_h^n &= \theta^n, \end{aligned} \tag{51}$$

then

$$u^n - u_h^n = u^n - R_h u^n + R_h u^n - u_h^n = \rho^n + \theta^n. \tag{52}$$

Theorem 9. *Assume that $u \in H^2(0,T;L_2(R)) \cap H^1(0,T;H_r(R))$. Then, there exists integers m $(1 \le m \le N)$ and constants C_0 and C_1 independent of the step parameters h and τ such that*

$$\begin{aligned} &\left\|u^m - u_h^m\right\|^2 + 2K\tau\sum_{i=1}^{m}\left|u^i - u_h^i\right|_r^2 \\ &\quad \le C_0\tau^2 + C_1 h^{2\{\min\{k+1,s\}-r\}} \end{aligned} \tag{53}$$

Here

$$\begin{aligned} C_0 &= C_0\left(\left\|u_{tt}\right\|^2_{L^2(0,T,L^2)}\right), \\ C_1 &= C_1\left(\left\|u_t\right\|_{L^2(0,T,H^s)}, \|u\|_{L^2(0,T,H^s)}\right). \end{aligned} \tag{54}$$

Proof. Take $v_h = \theta^n$ in (50) to obtain

$$\begin{aligned} &\left(\frac{\theta^n - \theta^{n-1}}{\tau}, \theta^n\right) + K\left\langle T_r\theta^n, \theta^n\right\rangle \\ &\quad + \frac{K}{\eta^2}\left(\left(R_h u^n\right)^3 - \left(u_h^n\right)^3, \theta^n\right) \\ &= \left(-S^n, \theta^n\right) + \left(\frac{\rho^{n-1} - \rho^n}{\tau}, \theta^n\right) \\ &\quad + \frac{K}{\eta^2}\left(\left(R_h u^n\right)^3 - \left(u^n\right)^3, \theta^n\right) + \frac{K}{\eta^2}\left(\rho^n, \theta^n\right) \\ &\quad + \frac{K}{\eta^2}\left(\theta^n, \theta^n\right). \end{aligned} \tag{55}$$

We first estimate the left-hand side of (55).

Applying the *Hölder* inequality and the Young inequality, we have

$$\begin{aligned} \left(\frac{\theta^n - \theta^{n-1}}{\tau}, \theta^n\right) &= \frac{1}{\tau}\left(\left(\theta^n, \theta^n\right) - \left(\theta^{n-1}, \theta^n\right)\right) \\ &\ge \frac{1}{\tau}\left(\left\|\theta^n\right\|^2 - \frac{\left\|\theta^{n-1}\right\|^2}{2} - \frac{\left\|\theta^n\right\|^2}{2}\right) \\ &= \frac{1}{2\tau}\left(\left\|\theta^n\right\|^2 - \left\|\theta^{n-1}\right\|^2\right). \end{aligned} \tag{56}$$

By using the monotonicity of function $((x_1)^3 - (x_2)^3)(x_1 - x_2) \ge 0$, we have

$$\begin{aligned} &\left(\left(R_h u^n\right)^3 - \left(u_h^n\right)^3, R_h u^n - u_h^n\right) \\ &\quad = \left(\left(R_h u^n\right)^3 - \left(u_h^n\right)^3, \theta^n\right) \ge 0. \end{aligned} \tag{57}$$

And then, we estimate the right-hand side of (55). Combining the *Hölder* inequality and the Young inequality, we have

$$\begin{aligned} \left(-S^n, \theta^n\right) &\le \left\|-S^n\right\|\left\|\theta^n\right\| \\ &= \frac{1}{\tau}\left\|\int_{t_{n-1}}^{t_n}\left(t - t_{n-1}\right)u_{tt}(t)\,dt\right\|\left\|\theta^n\right\| \\ &\le \frac{1}{\tau}\left(\int_0^1 \tau^3\int_{t_{n-1}}^{t_n} u_{tt}(t)\,dtdx\right)^{1/2}\left\|\theta^n\right\| \\ &= \tau^{1/2}\left(\int_{t_{n-1}}^{t_n}\left\|u_{tt}(t)\right\|^2 dt\right)^{1/2}\left\|\theta^n\right\| \\ &\le \tau\int_{t_{n-1}}^{t_n}\left\|u_{tt}(t)\right\|^2 dt + \left\|\theta^n\right\|^2. \end{aligned} \tag{58}$$

Similarly, we get

$$\begin{aligned} \left(\frac{\rho^{n-1} - \rho^n}{\tau}, \theta^n\right) &\le \left\|\frac{\rho^{n-1} - \rho^n}{\tau}\right\|\left\|\theta^n\right\| \\ &= \frac{1}{\tau}\left\|\int_{t_{n-1}}^{t_n}\rho_t(t)\,dt\right\|\left\|\theta^n\right\| \\ &\le \frac{1}{\tau^{1/2}}\left(\int_{t_{n-1}}^{t_n}\left\|\rho_t(t)\right\|^2 dt\right)^{1/2}\left\|\theta^n\right\| \\ &\le \frac{1}{2\tau}\int_{t_{n-1}}^{t_n}\left\|\rho_t(t)\right\|^2 dt + \frac{1}{2}\left\|\theta^n\right\|^2. \end{aligned} \tag{59}$$

The third term on the right-hand side of (55) is estimated by

$$\begin{aligned} \left(\left(R_h u^n\right)^3 - \left(u^n\right)^3, \theta^n\right) &\le C_1\left\|\rho^n\right\|\left\|\theta^n\right\| \\ &\le \frac{C_1}{2}\left\|\rho^n\right\|^2 + \frac{C_1}{2}\left\|\theta^n\right\|^2 \end{aligned} \tag{60}$$

and

$$\left(\rho^n, \theta^n\right) \le \left\|\rho^n\right\|\left\|\theta^n\right\| \le \frac{1}{2}\left\|\rho^n\right\|^2 + \frac{1}{2}\left\|\theta^n\right\|^2. \tag{61}$$

Then, taking these inequalities into (55), we obtain

$$\begin{aligned}&\left\|\theta^n\right\|^2-\left\|\theta^{n-1}\right\|^2+2K\tau\left|\theta^n\right|_r^2\\&\le\tau^2\int_{t_{n-1}}^{t_n}\left\|u_{tt}(t)\right\|^2dt+\int_{t_{n-1}}^{t_n}\left\|\rho_t(t)\right\|^2dt\\&\quad+\frac{(C_1+1)K}{\eta^2}\tau\left\|\rho^n\right\|^2\\&\quad+\left(2+\frac{C_1+3K}{\eta^2}\right)\tau\left\|\theta^n\right\|^2.\end{aligned}\tag{62}$$

Noticing $\theta^0=u_h^0-R_hu_0=0$ and adding all the terms from $n=1$ to $n=N$, we have

$$\begin{aligned}\left\|\theta^m\right\|^2+2K\tau\sum_{i=1}^m\left|\theta^i\right|_r^2&\le\tau^2\int_0^T\left\|u_{tt}(t)\right\|^2dt\\&\quad+\int_0^T\left\|\rho_t(t)\right\|^2dt\\&\quad+\frac{C_1K+K}{\eta^2}\tau\sum_{i=1}^N\left\|\rho^i\right\|^2\\&\quad+\frac{2\eta^2+C_1+3K}{\eta^2}\tau\sum_{i=1}^N\left\|\theta^i\right\|^2.\end{aligned}\tag{63}$$

The discrete Gronwall inequality is applied to (63), when τ is small enough to satisfy $((2\eta^2+C_1+3K)/\eta^2)\tau<1$,

$$\begin{aligned}&\left\|\theta^m\right\|^2+2K\tau\sum_{i=1}^m\left|\theta^i\right|_r^2\\&\le e^{(2\eta^2+C_1+3K)T/\eta^2}\left(\tau^2\int_0^T\left\|u_{tt}(t)\right\|^2dt\right.\\&\left.\quad+\int_0^T\left\|\rho_t(t)\right\|^2dt+\frac{C_1K+K}{\eta^2}\tau\sum_{i=1}^N\left\|\rho^i\right\|^2\right).\end{aligned}\tag{64}$$

If we take $C=\max\{(1/3)e^{(2\eta^2+C_1+3K)T/\eta^2},e^{(2\eta^2+C_1+3K)T/\eta^2},((C_1K+K)/\eta^2)e^{(2\eta^2+C_1+3K)T/\eta^2}\}$, then

$$\begin{aligned}\left\|\theta^m\right\|^2+2K\tau\sum_{i=1}^m\left|\theta^i\right|_r^2&\le C\tau^2\left\|u_{tt}\right\|_{L^2(0,T,L^2)}^2\\&\quad+Ch^{2\min\{k+1,s\}}\left\|u_t\right\|_{L^2(0,T,H^s)}^2\\&\quad+Ch^{2\min\{k+1,s\}}\left\|u\right\|_{L^2(0,T,H^s)}^2.\end{aligned}\tag{65}$$

Then, using the elliptic projection estimate (49) and the triangle inequality, we obtain

$$\begin{aligned}&\left\|u^m-u_h^m\right\|^2+2K\tau\sum_{i=1}^m\left|u^i-u_h^i\right|_r^2\\&\le\left\|\rho^m\right\|^2+\left\|\theta^m\right\|^2+2K\tau\sum_{i=1}^m\left|\theta^i\right|_r^2+2K\tau\sum_{i=1}^m\left|\rho^i\right|_r^2\\&\le C_0\tau^2+C_1h^{2\{\min\{k+1,s\}-r\}}.\end{aligned}\tag{66}$$

This concludes the proof. □

Remark 10. Since our proof for the stability, energy dissipation, new energy-equality and error deduction of the discrete scheme (15) is independent of the dimensional argument, the analysis and conclusions in this article can be extended to multidimensional models, maybe with minor modification.

6. Fast-Conjugate-Gradient Algorithm (FCG)

The fully discrete finite element scheme (15) is nonlinear and can be solved by Newton's iteration algorithm. Here we linearize the nonlinear terms by replacing $(u_h^n)^2$ by $(u_h^{n-1})^2$ and solve this linearized version by the conjugated gradient algorithm (CG). We find that if the CG algorithm is directly used, the computation cost and storage will reach up to $\mathcal{O}(M^2)$ since the coefficient matrix B is nonsparse due to the nonlocality of the fractional Laplace operator. We also find that if the linear finite element space is employed, the matrix B is a Toeplitz matrix (see Section 7.1), which makes it possible to reduce the computation cost and storage to $\mathcal{O}(M\log M)$ by a delicate combination of the CG algorithm, the fast Fourier transform (FFT) and its Toeplitz structure of the matrix B.

In this section, we depict the general ideas for the combination of CG, FFT, and the Toeplitz matrix and design a fast CG algorithm (FCG). For a good review of a fast algorithm generating from FFT and the Toeplitz matrix, we refer to [28].

Noticing what causes the computation cost up to $O(M^2)$ is a direct use of the matrix-vector multiplication in the classical CG algorithm; as a remedy, we can obtain the matrix-vector multiplication $B_{kM-1}\mathbf{x}$ for a vector $x\in R^{kM-1}$ and $(kM-1)\times(kM-1)$ Toeplitz matrix B_{kM-1} through the following two steps [29, 30]:

(1) assembling the $(kM-1)\times(kM-1)$ Toeplitz matrix B_{kM-1} into a $2(kM-1)\times2(kM-1)$ cyclic matrix $C_{2(kM-1)}$;

(2) extracting the Toeplitz matrix-vector multiplication $B_{kM-1}\mathbf{x}$ for a vector $x\in R^{kM-1}$ via

$$C_{2(kM-1)}\mathbf{X}=\begin{pmatrix}B_{kM-1}&D_{kM-1)}\\D_{kM-1}&B_{kM-1}\end{pmatrix}\begin{pmatrix}\mathbf{x}\\\mathbf{0}\end{pmatrix}=\begin{pmatrix}B_{kM-1}\mathbf{x}\\D_{kM-1}\mathbf{x}\end{pmatrix}.\tag{67}$$

In (67), D_{kM-1} is determined simply by the matrix B_{kM-1} and the computational cost and the storage of the matrix-vector multiplication $B_{kM-1}\mathbf{x}$ are $O(M\log M)$ and $O(M)$ [30]. This will reduce the computation cost and the storage from $\mathcal{O}(M^2)$ to $O(M\log M)$ and $O(M)$ compared to the direct use of matrix-vector multiplication.

Upon this analysis, we write down the improved algorithm, called the fast CG (FCG), sentence by sentence in Algorithm 1, and present the corresponding conclusion by Theorem 11.

Theorem 11. *The computational cost and storage of the fast conjugated gradient algorithm (FCG) are reduced from $O(M^2)$ and $O(M^2)$ to $O(M\log M)$ and $O(M)$ compared with the traditional CG algorithm.*

```
function FCG(F, U)
  rb = F − F_T(U);
  nr = norm(rb);
  k = 0;
  ρ = rb′ ∗ rb;
  while 1
  k = k + 1;
   if k == 1 then
     p = rb;
     else
     β = ρ/ρ_wave;
     p = rb + β ∗ p;
   end if
  w = F_T(p);
   α = ρ/(w′ ∗ p);
   U = U + α ∗ p;
   rb = rb − α ∗ w;
   ρ_wave = ρ;
  ρ = rb′ ∗ rb;
  if sqrt(rho) > e^−7 then
    continue;
   else
    break;
  end if
end function
```

Algorithm 1: The FCG Algorithm.

7. Numerical Experiments

In this section, we linearize the nonlinear term in the fully discrete finite element scheme (15) by taking $(u_h^{n-1})^2 u_h^n$ to replace $(u_h^n)^3$; we carry out two numerical experiments to verify the result convergence analysis and the physical property of the solution of discrete system.

7.1. The Linear Finite Element System. For simplicity, we take the linear finite element system to compute algebraic equation (17).

For $k = 1$, the inner nodal basis function is $\varphi_i(x)$ at x_i, $i = 1, 2, \ldots, M-1$, with the following structure:

$$\varphi_i(x) = \begin{cases} \dfrac{x - x_{i-1}}{h}, & x \in (x_{i-1}, x_i), \\ \dfrac{x_{i+1} - x}{h}, & x \in (x_i, x_{i+1}), \\ 0, & else. \end{cases} \tag{68}$$

For $i, j = 1, 2, \ldots, M-1$, the matrix A is

$$A = \left[\left(\varphi_i, \varphi_j\right)\right]_{(M-1)\times(M-1)}$$

$$= \begin{pmatrix} \frac{2h}{3} & \frac{h}{6} & 0 & \cdots & 0 \\ \frac{h}{6} & \frac{2h}{3} & \frac{h}{6} & \cdots & 0 \\ \vdots & \ddots & \ddots & \ddots & \vdots \\ 0 & \ddots & \ddots & \frac{2h}{3} & \frac{h}{6} \\ 0 & 0 & \cdots & \frac{h}{6} & \frac{2h}{3} \end{pmatrix}. \tag{69}$$

We replace the nonlinear term $H(U^n)$ with $H(U^{n-1})$,

$$H\left(U^{n-1}\right) = \left[\left(\left(u_h^{n-1}\right)^2 \varphi_i, \varphi_j\right)\right]_{(M-1)\times(M-1)}, \quad i, j = 1, 2, \ldots, M-1. \tag{70}$$

After calculation, the ij–entries of the matrix $H(U^{n-1})$ are

$$\left(\left(u_h^{n-1}\right)^2 \varphi_i, \varphi_j\right) = \begin{cases} \dfrac{\left(u_{i-1}^{n-1}\right)^2}{30} + \dfrac{2\left(u_i^{n-1}\right)^2}{5} + \dfrac{u_{i-1}^{n-1}u_i^{n-1} + u_i^{n-1}u_{i+1}^{n-1}}{10} + \dfrac{\left(u_{i+1}^{n-1}\right)^2}{30}, & |j-i| = 0, \\ \dfrac{\left(u_i^{n-1}\right)^2}{20} + \dfrac{\left(u_j^{n-1}\right)^2}{20} + \dfrac{u_i^{n-1}u_j^{n-1}}{15}, & |j-i| = 1, \\ 0, & |j-i| = m, m = 2, \ldots, M-2. \end{cases} \tag{71}$$

For $i, j = 1, 2, \ldots, M-1$, the entries of the matrix B are respectively

$$\left\langle T_r\varphi_i, \varphi_j \right\rangle = \frac{C_r}{2} \int_R \int_R \frac{\left(\varphi_i(x) - \varphi_i(y)\right)\left(\varphi_j(x) - \varphi_j(y)\right)}{|x-y|^{1+2r}} dxdy$$

$$= \frac{C_r}{2}\left\{\int_\Omega\int_{R\setminus\Omega}\frac{(\varphi_i(x)-\varphi_i(y))(\varphi_j(x)-\varphi_j(y))}{|x-y|^{1+2r}}dxdy + \int_{R\setminus\Omega}\int_\Omega\frac{(\varphi_i(x)-\varphi_i(y))(\varphi_j(x)-\varphi_j(y))}{|x-y|^{1+2r}}dxdy + \int_\Omega\int_\Omega\frac{(\varphi_i(x)-\varphi_i(y))(\varphi_j(x)-\varphi_j(y))}{|x-y|^{1+2r}}dxdy\right\}. \tag{72}$$

After calculating the above integrals (72), we obtain that the ij–entries of matrix B are solved for $r \neq 1/2$

$$\left\langle T_r\varphi_i,\varphi_j\right\rangle = \begin{cases} \frac{h^{1-2r}}{D}\left\{-4+2^{3-2r}\right\}, & |j-i|=0,\\ \frac{h^{1-2r}}{D}\left\{\frac{7}{2}-2^{4-2r}+\frac{3^{3-2r}}{2}\right\}, & |j-i|=1,\\ \frac{h^{1-2r}}{D}\left\{3m^{3-2r}-2(m+1)^{3-2r}-2(m-1)^{3-2r}+\frac{(m-2)^{3-2r}}{2}+\frac{(m+2)^{3-2r}}{2}\right\}, & |j-i|=m, m=2,\ldots,M-2, \end{cases} \tag{73}$$

where

$$D = \frac{r(1-2r)(2-2r)(3-2r)}{C_r}, \qquad C_r = \frac{4^r r\Gamma(1/2+r)}{\pi^{1/2}\Gamma(1-r)}. \tag{74}$$

For $r = 1/2$,

$$\left\langle T_r\varphi_i,\varphi_j\right\rangle = \begin{cases} 4C_r\ln 2, & |\mathrm{j}-\mathrm{i}|=0,\\ C_r\left(\frac{7}{2}\ln 3-\ln 2\right), & |\mathrm{j}-\mathrm{i}|=1,\\ C_r(14\ln 2-9\ln 3), & |\mathrm{j}-\mathrm{i}|=2,\\ C_r\left\{3m^2\ln(\mathrm{m})+\frac{(\mathrm{m}-2)^2}{2}\ln(\mathrm{m}-2)+\frac{(m+2)^2}{2}\ln(\mathrm{m}+2)-2(\mathrm{m}-1)^2\ln(\mathrm{m}-1)-2(m+1)^2\ln(\mathrm{m}+1)\right\}, & |\mathrm{j}-\mathrm{i}|=\mathrm{m},\ \mathrm{m}=3,\ldots,\mathrm{M}-2. \end{cases} \tag{75}$$

7.2. Tests on the Efficiency of the Finite Element Procedure and the FCG

Example 12. Assuming $\Omega = [0,1], T = 1, K = 1$, the analytic solution is

$$u(x,t) = x(1-x)e^t \in H_0^{1+\gamma}(\Omega), \tag{76}$$

where $\gamma \in (0,1/2)$, is selected as close to $1/2$ as possible. The source term f should be expressed as follows:

$$f = x(1-x)e^t + KC_r\left[\frac{x^{1-2r}e^t}{2r(1-2r)}+\frac{(1-x)^{1-2r}e^t}{2r(1-2r)} - \frac{x^{2-2r}e^t}{r(1-2r)(2-2r)}-\frac{(1-x)^{2-2r}e^t}{r(1-2r)(2-2r)}\right] + \frac{K}{\eta^2}\left[x^3(1-x)^3e^t - x(1-x)e^t\right]. \tag{77}$$

We apply Example 12 to verify the error convergence rate of the linear finite element system and to test the efficiency of the FCG for $r = 1/3, 2/3$.

The numerical solution $U_h(x)$ is calculated by the FCG for $T = 1$. The numerical solution and the exact solution are identical at $t = 1$ in Figure 1, which show that the FCG is accurate.

Table 1: Spatial errors and convergence rates for $\|u - u_h\|_{H_{r,0}}$.

r	h	Newton	rate	Gauss	rate	CG	rate	FCG	rate
$\frac{1}{3}$	2^{-3}	1.247E-2		1.336E-2		1.336E-2		1.336E-2	
	2^{-4}	4.026E-3	1.63	4.204E-3	1.66	4.204E-3	1.66	4.204E-3	1.66
	2^{-5}	1.276E-3	1.65	1.312E-3	1.67	1.312E-3	1.67	1.312E-3	1.67
	2^{-6}	4.047E-4	1.65	4.121E-4	1.67	4.121E-4	1.67	4.121E-4	1.67
	2^{-7}	1.299E-4	1.63	1.313E-4	1.64	1.313E-4	1.64	1.313E-4	1.64
$\frac{2}{3}$	2^{-3}	4.260E-2		4.294E-2		4.294E-2		4.294E-2	
	2^{-4}	1.808E-2	1.23	1.814E-2	1.24	1.814E-2	1.24	1.814E-2	1.24
	2^{-5}	7.544E-3	1.26	7.556E-3	1.26	7.556E-3	1.26	7.556E-3	1.26
	2^{-6}	3.164E-3	1.25	3.167E-3	1.25	3.167E-3	1.25	3.167E-3	1.25
	2^{-7}	1.361E-3	1.21	1.362E-3	1.21	1.362E-3	1.21	1.362E-3	1.21

Table 2: Spatial errors and convergence rates for $\|u - u_h\|$.

r	h	Newton	rate	Gauss	rate	CG	rate	FCG	rate
$\frac{1}{3}$	2^{-3}	6.117E-3		7.269E-3		7.270E-3		7.434E-3	
	2^{-4}	1.755E-3	1.80	2.031E-3	1.84	2.030E-3	1.84	2.060E-3	1.85
	2^{-5}	4.800E-4	1.87	5.476E-4	1.89	5.475E-4	1.89	5.540E-4	1.89
	2^{-6}	1.286E-4	1.90	1.451E-4	1.92	1.451E-4	1.92	1.468E-4	1.92
	2^{-7}	3.434E-5	1.90	3.834E-5	1.92	3.833E-5	1.92	3.891E-5	1.92
$\frac{2}{3}$	2^{-3}	6.517E-3		7.322E-3		7.321E-3		7.497E-3	
	2^{-4}	2.220E-3	1.55	2.411E-3	1.60	2.414E-3	1.60	2.452E-3	1.61
	2^{-5}	7.480E-4	1.56	7.937E-4	1.60	7.937E-4	1.60	8.050E-4	1.60
	2^{-6}	2.567E-4	1.54	2.675E-4	1.56	2.675E-4	1.56	2.711E-4	1.57
	2^{-7}	9.084E-5	1.49	9.340E-5	1.51	9.340E-5	1.51	9.455E-5	1.51

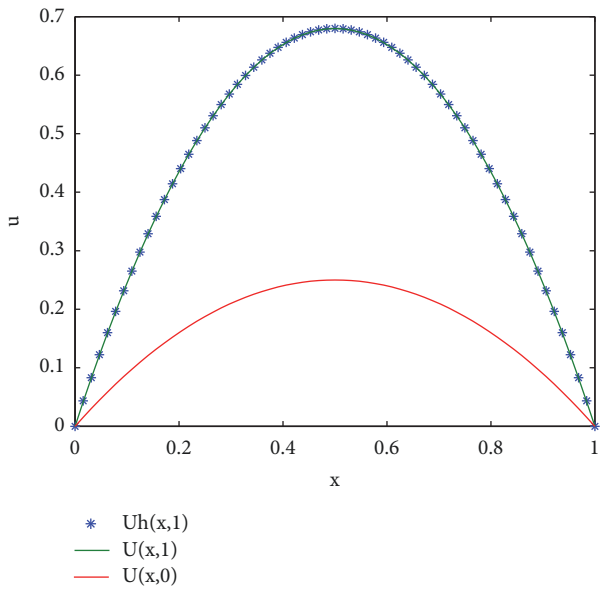

Figure 1: Comparison of the initial value, the exact solution, and the numerical solution for $r = 1/3, K = 1, \eta = 1$.

Table 1 show the spatial convergence rates with respect to $\|u - u_h\|_{H_0^r}$ for $r = 1/3, 2/3$ respectively. By comparing the convergence rates of FCG to the convergence rate of Newton, Gauss, and CG, respectively, we conclude that the FCG algorithm is efficient. The convergence rates of $\|u - u_h\|_{H_0^r}$ are at least 1.6 and 1.2 for $r = 1/3, 2/3$, respectively, which are almost equal to the theoretical error rate $\min\{1 + \gamma, 2\} - r$.

Table 2 shows the spatial convergence rates with respect to $\|u-u_h\|$ for $r = 1/3, 2/3$, respectively. The convergence rates of $\|u-u_h\|$ are at least 1.9 and 1.5 for $r = 1/3, 2/3$, respectively. We observe that the spatial convergence rates decrease as the spatial fractional order r increases.

Remark 13. Recalling L_2 error estimate for second order elliptic equation, one can obtain the estimate of $\|u - u_h\|$ one order higher than that for $|u - u_h|_1$. However, in the case of the fractional order elliptic equation, we only obtain the convergence rate of $\|u - u_h\|$ dependent on the index r. From the numerical Table 2, the convergence order of $\|u-u_h\|$ conforms to the following relation.

Table 3: Temporal errors and convergence rates.

r	τ	Newton	rate	Gauss	rate	CG	rate	FCG	rate
$\frac{1}{3}$	$\frac{1}{8}$	1.173E-2		2.245E-2		2.245E-2		2.246E-2	
	$\frac{1}{10}$	6.012E-3	0.96	1.788E-2	1.020	1.788E-2	1.020	1.788E-2	1.020
	$\frac{1}{12}$	3.044E-3	0.98	1.486E-2	1.017	1.486E-2	1.017	1.486E-2	1.017
	$\frac{1}{14}$	1.532E-3	0.99	1.270E-2	1.014	1.270E-2	1.014	1.270E-2	1.014
	$\frac{1}{16}$	7.696E-4	0.99	1.110E-2	1.012	1.110E-2	1.012	1.110E-2	1.012
$\frac{2}{3}$	$\frac{1}{8}$	6.768E-3		1.375E-2		1.376E-2		1.376E-2	
	$\frac{1}{10}$	3.478E-3	0.96	1.103E-2	0.988	1.103E-2	0.989	1.103E-2	0.988
	$\frac{1}{12}$	1.766E-3	0.97	9.210E-3	0.991	9.211E-3	0.991	9.211E-3	0.991
	$\frac{1}{14}$	8.935E-4	0.98	7.904E-3	0.992	7.904E-3	0.992	7.904E-3	0.992
	$\frac{1}{16}$	4,527E-4	0.98	6.922E-3	0.993	6.922E-3	0.993	6.922E-3	0.993

Table 4: CPU time of Newton, Gauss, CG, and FCG.

	h	Newton	Gauss	CG	FCG
$r = 1/3$	2^{-5}	0.38s	0.25s	0.22s	0.34s
	2^{-6}	5.11s	8.22s	2.14s	1.12s
	2^{-7}	1.1m	3.77m	16.63s	4.94s
	2^{-8}	19.3m	1.94h	2.27m	14.71s
	2^{-9}	5.19h	69.9h	23.6m	1.74m
	2^{-10}	15.2h	-	6.79h	25.35m

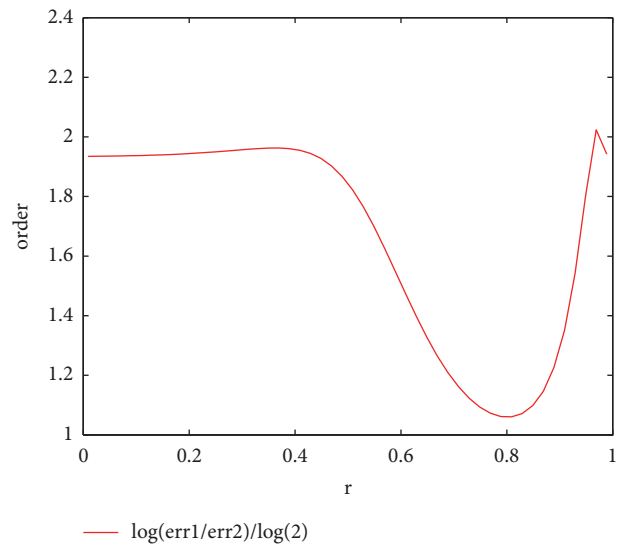

Figure 2: The relation of spatial convergence rates and fractional order r.

Figure 2 shows that the convergence rate of $\|u - u_h\|$ dependent on the index r, as the index r increases, the rates of spatial convergence decreases and then increases.

Table 3 shows the temporal convergence rates as $r = 1/3, r = 2/3$, respectively. The temporal convergence rates are almost equal to 1 for $r = 1/3, r = 2/3$ at $h = 2^{-10}$, which are consistent with the theoretical expectation for the backward Euler scheme.

Table 4 shows the efficiency of the FCG algorithm. It is easily obtained that the CPU time consumed by the FCG is much less than that of the Newton, Gauss, and CG as h decreases. It can be seen that the CPU time of FCG is 25.35 minutes while the Newton's 15.2 hours and the CG's 6.79 hours for $h = 2^{-10}$, $r = 1/3$. These show that the FCG is an efficiency algorithm.

7.3. Tests on Physical Properties of Finite Element Solution

Example 14. Letting $h = 1/100$, $\tau = 1/500$, the initial value is

$$u(x, 0) = 0.9 \sin(2\pi x). \quad (78)$$

This example is used to test the physical properties such as the energy laws and the new energy equality, the mass dissipation, the phase separation, and the tunable sharpness in Figures 3–8.

We present the energy dissipation in Figure 3 and the new energy equality in Figure 4 for $r = 0.3$, $\eta = 0.85$, and $K = 1$. In Figure 3, the energy dissipates to zero as time increases. In

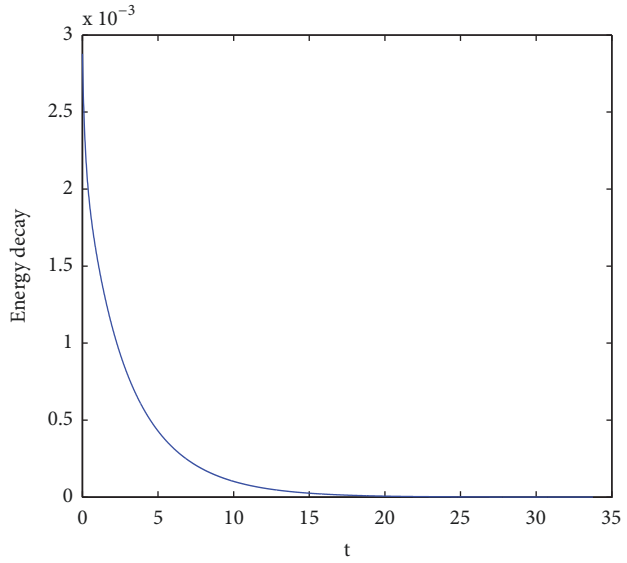

Figure 3: Energy dissipation with time increasing.

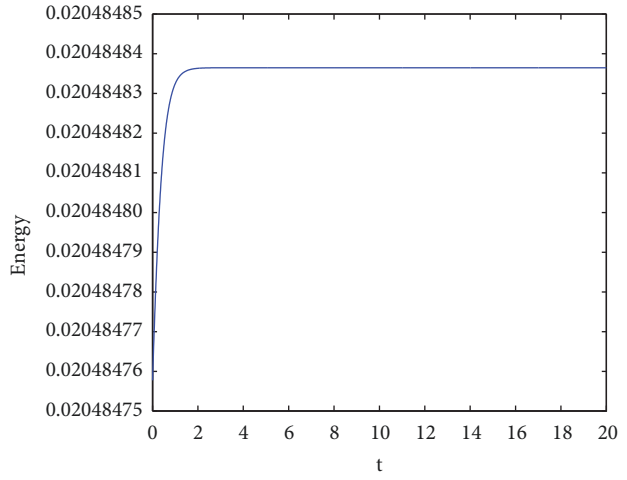

Figure 4: The new energy equality for $r = 0.3$, $\eta = 0.85$, and $K = 1$.

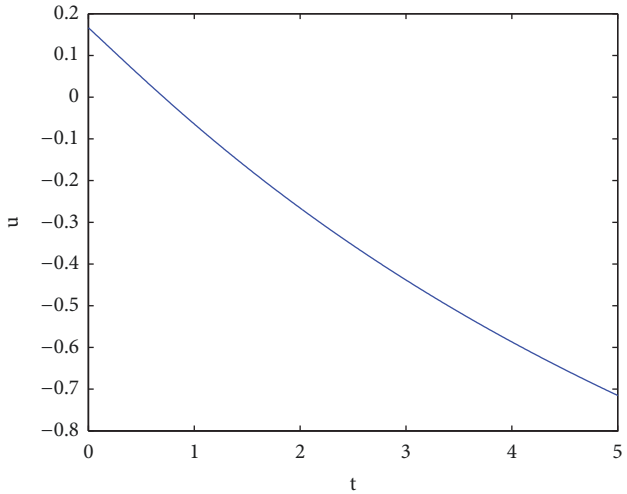

Figure 5: The mass dissipation for $r = 0.3$, $\eta = 0.85$, and $K = 1$.

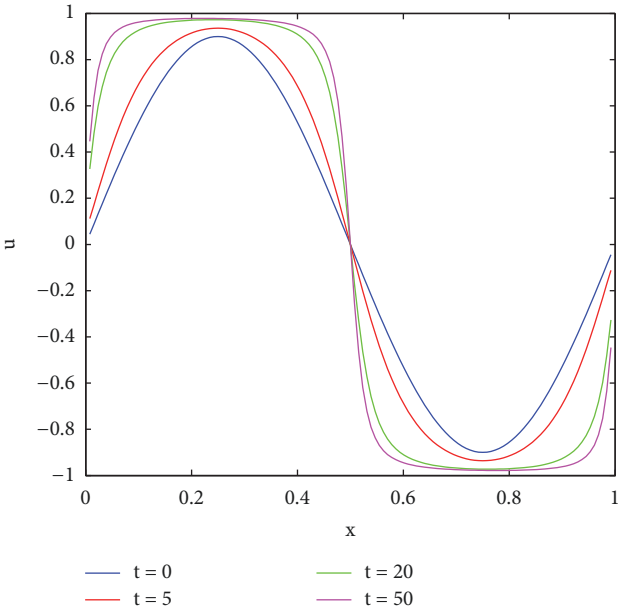

Figure 6: The coarse graining process with respect to different t.

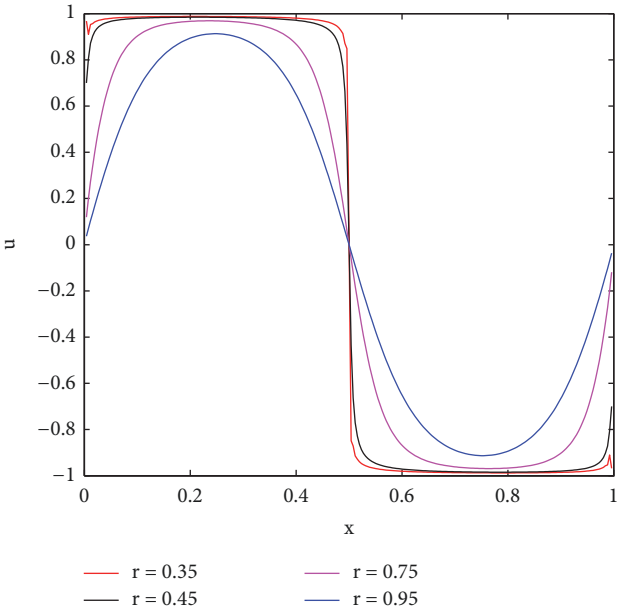

Figure 7: The tunable sharpness with respect to different r.

Figure 4, the energy jumps in scale 10^{-7} at the beginning until $t = 1$ and keeps the same at the end; this demonstrates that the finite element solution to (15) almost satisfies new equality equation.

We plot the mass changes for $r = 0.3$, $\eta = 0.85$, and $K = 1$ in Figure 5. The mass value dissipates as time increases; this property is coinciding with the classical Allen-Cahn equation, and this also explains the applicability of fractional Laplacian for Allen-Cahn equation in some way.

We present the physical phenomenon of a coarse graining process as the time increases for $r = 0.6$, $\eta = 0.1$, and $K =$

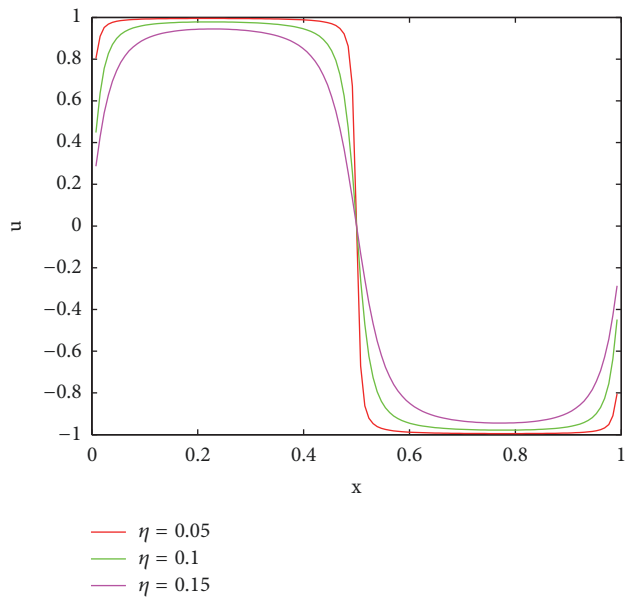

Figure 8: The tunable sharpness with respect to different η.

0.001 in Figure 6. The two phases are connected in a smooth steep line; this indicates that the phase separation is complete.

Figure 7 shows that the interface gets sharper and sharper as r decreases. Figure 8 shows that the interface gets sharper and sharper as η decreases. The above two groups of experimental results show that the tunable sharpness of the interface is related to different parameters r and η.

Data Availability

The data used to support the findings of this study are available from the corresponding author upon request.

Conflicts of Interest

The authors declare no conflicts of interest regarding the publication of this paper.

Acknowledgments

This work is supported in part by the National Natural Science Foundation of China under Grant nos. 11471196, 10971254, and 11471194.

References

[1] S. M. Allen and J. W. Cahn, "A microscopic theory for antiphase boundary motion and its application to antiphase domain coarsening," *Acta Metallurgica et Materialia*, vol. 27, no. 6, pp. 1085–1095, 1979.

[2] X. Yang, J. J. Feng, C. Liu, and J. Shen, "Numerical simulations of jet pinching-off and drop formation using an energetic variational phase-field method," *Journal of Computational Physics*, vol. 218, no. 1, pp. 417–428, 2006.

[3] Q. Du, C. Liu, and X. Q. Wang, "A phase field approach in the numerical study of the elastic bending energy for vesicle membranes," *Journal of Computational Physics*, vol. 198, no. 2, pp. 450–468, 2004.

[4] L. C. Evans and J. Spruck, "Motion of level sets by mean curvature I," *Journal of Geometric Analysis*, vol. 33, no. 3, pp. 635–681, 1991.

[5] L. C. Evans, H. M. Soner, and P. E. Souganidis, "Phase transitions and generalized motion by mean curvature," *Communications on Pure and Applied Mathematics*, vol. 45, no. 9, pp. 1097–1123, 1992.

[6] C. Liu and J. Shen, "A phase field model for the mixture of two incompressible fluids and its approximation by a Fourier-spectral method," *Physica D: Nonlinear Phenomena*, vol. 179, no. 3-4, pp. 211–228, 2003.

[7] P. Yue, J. J. Feng, C. Liu, and J. Shen, "Diffuse-interface simulations of drop coalescence and retraction in viscoelastic fluids," *Journal of Non-Newtonian Fluid Mechanics*, vol. 129, no. 3, pp. 163–176, 2005.

[8] P. Yue, C. Zhou, J. J. Feng, C. F. Ollivier-Gooch, and H. H. Hu, "Phase-field simulations of interfacial dynamics in viscoelastic fluids using finite elements with adaptive meshing," *Journal of Computational Physics*, vol. 219, no. 1, pp. 47–67, 2006.

[9] M. Plapp, "Phase-field models," *CISM International Centre for Mechanical Sciences, Courses and Lectures*, vol. 538, pp. 129–175, 2012.

[10] J. Shen, "Modeling and numerical approximation of two-phase incompressible flows by a phase-field approach," in *Multiscale Modeling and Analysis for Materials Simulation*, vol. 22, pp. 147–195, 2012.

[11] Y. Wang and J. Li, "Phase field modeling of defects and deformation," *Acta Materialia*, vol. 58, no. 4, pp. 1212–1235, 2010.

[12] M. Beneš, V. Chalu, and K. Mikula, "Geometrical image segmentation by the allen-cahn equation," *Applied Numerical Mathematics*, vol. 51, no. 2-3, pp. 187–205, 2004.

[13] X. Feng and A. Prohl, "Numerical analysis of the Allen-Cahn equation and approximation for mean curvature flows," *Numerische Mathematik*, vol. 94, no. 1, pp. 33–65, 2003.

[14] J. Shen and X. Yang, "Numerical approximations of Allen-Cahn and Cahn-Hilliard equations," *Discrete and Continuous Dynamical Systems - Series A*, vol. 28, no. 4, pp. 1669–1691, 2010.

[15] S. Zhai, Z. F. Weng, and X. L. Feng, "Fast explicit operator splitting method and time-step adaptivity for fractional non-local Allen-Cahn model," *Applied Mathematical Modelling: Simulation and Computation for Engineering and Environmental Systems*, vol. 40, no. 2, pp. 1315–1324, 2016.

[16] Y. Nec, A. A. Nepomnyashchy, and A. A. Golovin, "Front-type solutions of fractional allen-cahn equation," *Physica D: Nonlinear Phenomena*, vol. 237, no. 24, pp. 3237–3251, 2008.

[17] F. Song, C. Xu, and G. E. Karniadakis, "A fractional phase-field model for two-phase flows with tunable sharpness: Algorithms and simulations," *Computer Methods Applied Mechanics and Engineering*, vol. 305, pp. 376–404, 2016.

[18] T. Hou, T. Tang, and J. Yang, "Numerical analysis of fully discretized crank–nicolson scheme for fractional-in-space allen–cahn equations," *Journal of Scientific Computing*, vol. 72, no. 3, pp. 1214–1231, 2017.

[19] A. M. Chen and F. W. Liu, "A finite volume unstructured mesh method for fractional-in-space Allen-Cahn equation," *Chinese Quarterly Journal of Mathematics*, vol. 32, no. 4, pp. 345–354, 2017.

[20] Z. Li, H. Wang, and D. Yang, "A space–time fractional phase-field model with tunable sharpness and decay behavior and its efficient numerical simulation," *Journal of Computational Physics*, vol. 347, pp. 20–38, 2017.

[21] R. Fletcher, "Conjugate gradient methods for indefinite systems," in *Numerical Analysis*, pp. 73–89, 1976.

[22] G. Akagi, G. Schimperna, and A. Segatti, "Fractional Cahn–Hilliard, Allen–Cahn and porous medium equations," *Journal of Differential Equations*, vol. 261, no. 6, pp. 2935–2985, 2016.

[23] E. D. Nezza, G. Palatucci, and E. Valdinoci, "Hitchhiker's guide to the fractional Sobolev spaces," *Bulletin des Sciences Mathématiques*, vol. 136, no. 5, pp. 521–573, 2012.

[24] R. A. Adams and J. J. Fournier, *Sobolev Spaces*, Elsevier, Amsterdam, Netherlands, 2003.

[25] V. J. Ervin and J. P. Roop, "Variational formulation for the stationary fractional advection dispersion equation," *Numerical Methods for Partial Differential Equations*, vol. 22, no. 3, pp. 558–576, 2010.

[26] J. Caristi, "Fixed point theorems for mappings satisfying inwardness conditions," *Transactions of the American Mathematical Society*, vol. 215, pp. 241–251, 1976.

[27] H. Chen and H. Wang, "Numerical simulation for conservative fractional diffusion equations by an expanded mixed formulation," *Journal of Computational and Applied Mathematics*, vol. 296, pp. 480–498, 2016.

[28] K. Wang and H. Wang, "A fast characteristic finite difference method for fractional advection-diffusion equations," *Advances in Water Resources*, vol. 34, no. 7, pp. 810–816, 2011.

[29] P. J. Davis, *Circulant Matrices*, Wiley Intersciences, 1979.

[30] R. M. Gray, "Toeplitz and circulant matrices: a review," *Foundations and Trends in Communication and Information Theory*, vol. 2, no. 3, pp. 155–239, 2006.